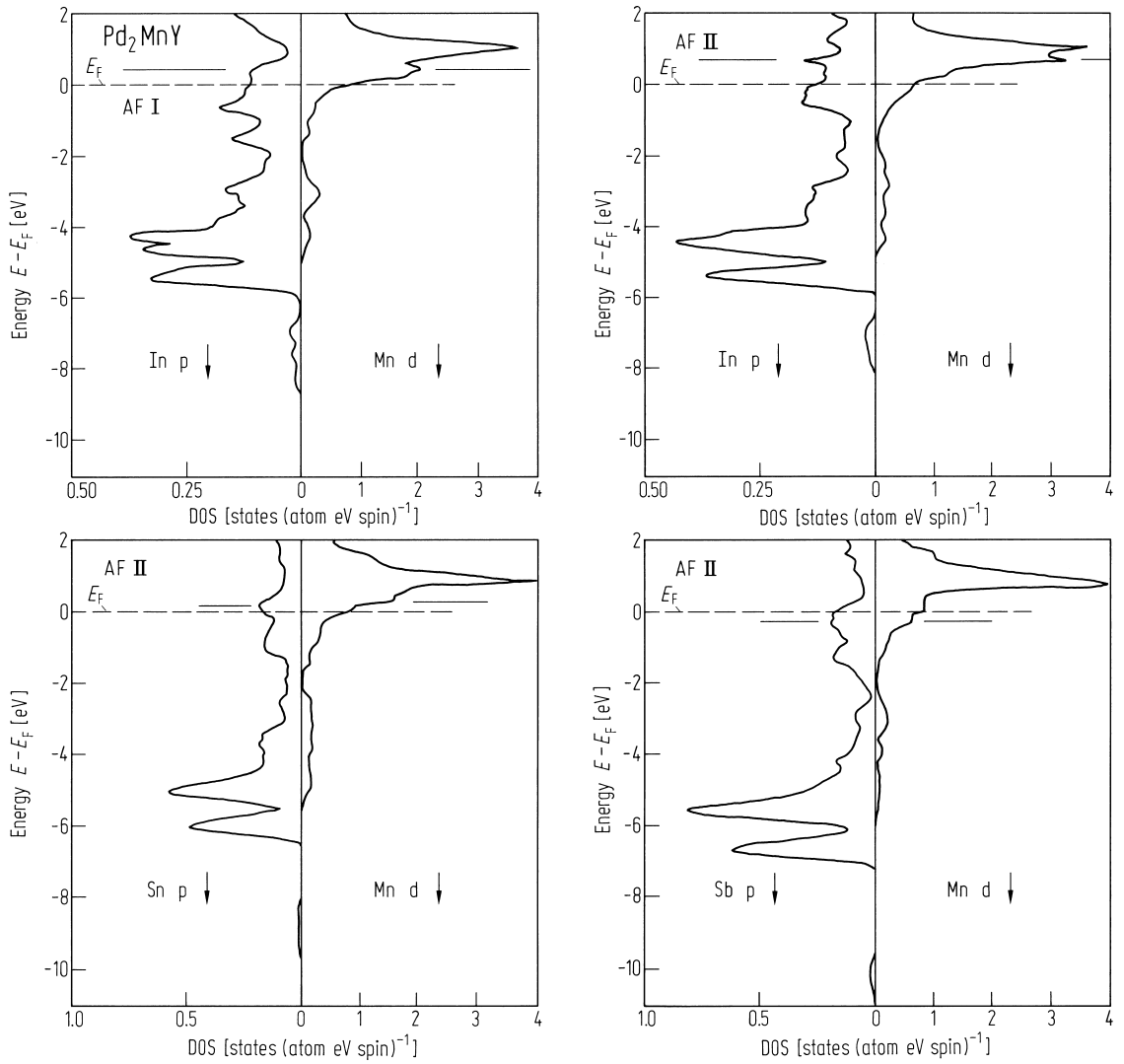

Fig. 513. Minority site- and spin-projected state densities of p and d electrons in antiferromagnetic Pd_2MnY. From left to right: Y = In in AF I order then in AF II order; Y = Sn in AF II order; Y = Sb in AF II order [83K4].

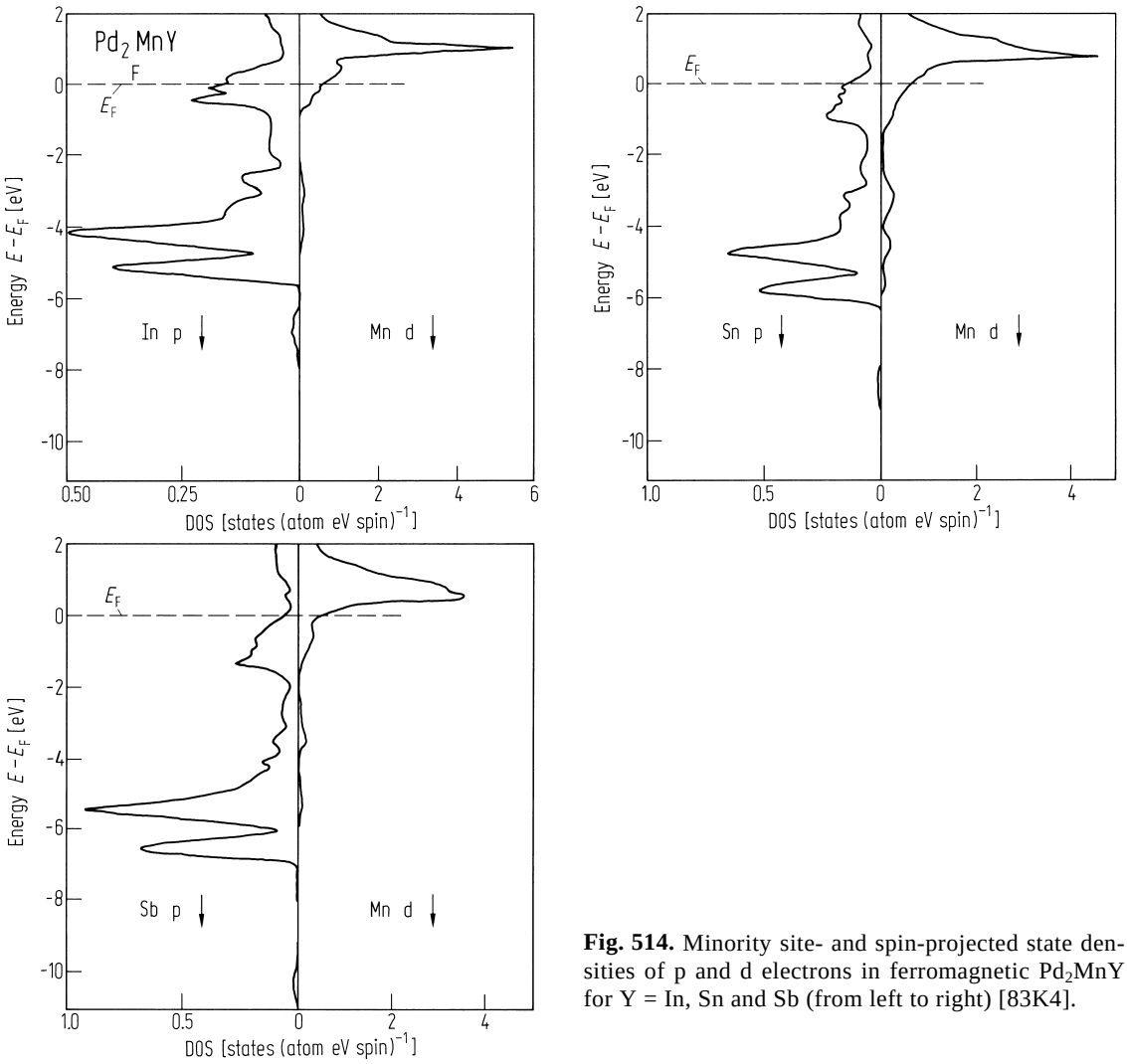

Fig. 514. Minority site- and spin-projected state densities of p and d electrons in ferromagnetic Pd_2MnY for Y = In, Sn and Sb (from left to right) [83K4].

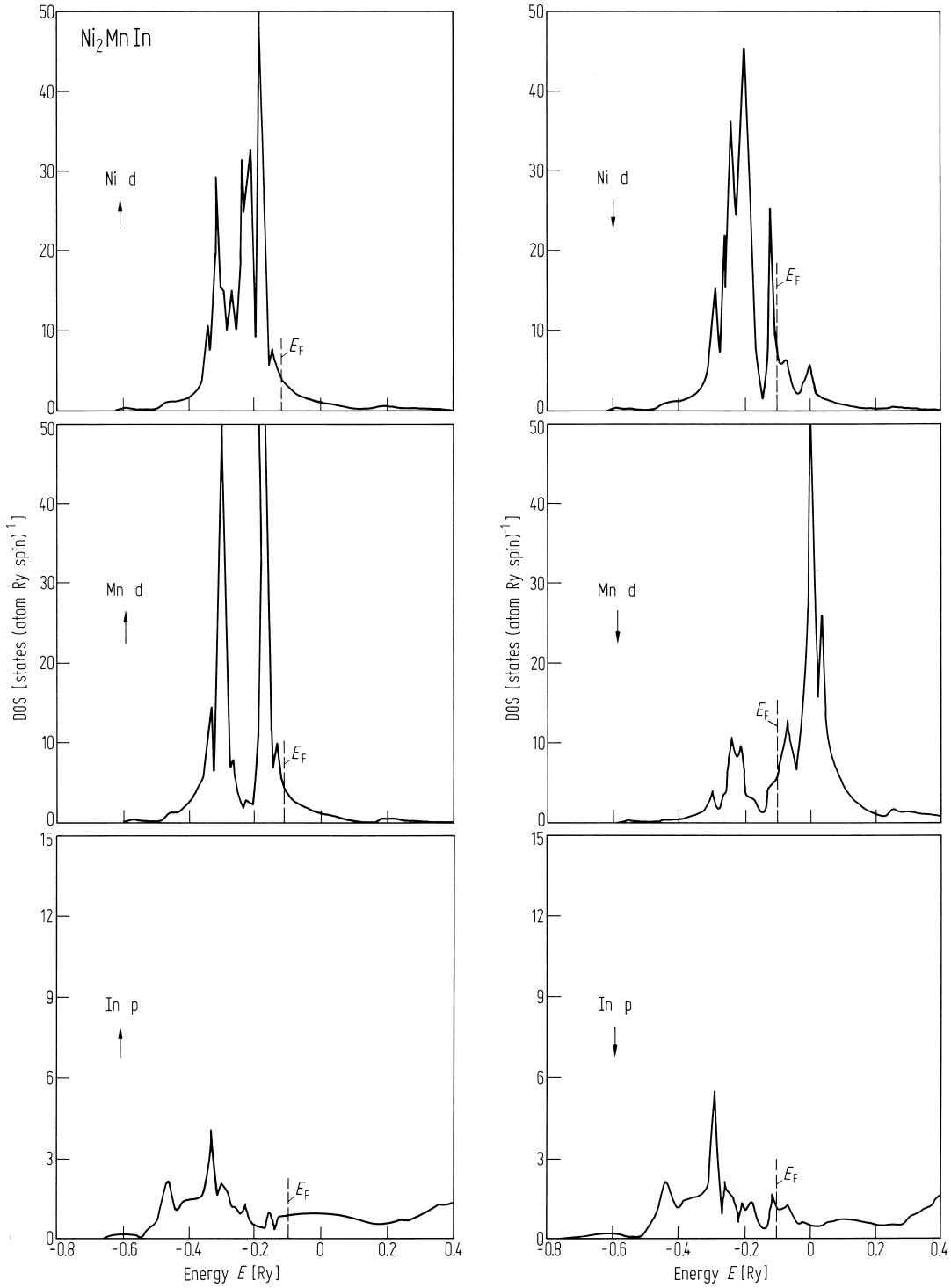

Fig. 515. Ni-d , Mn-d and In-p projected densities of states for Ni_2MnIn [88D1].

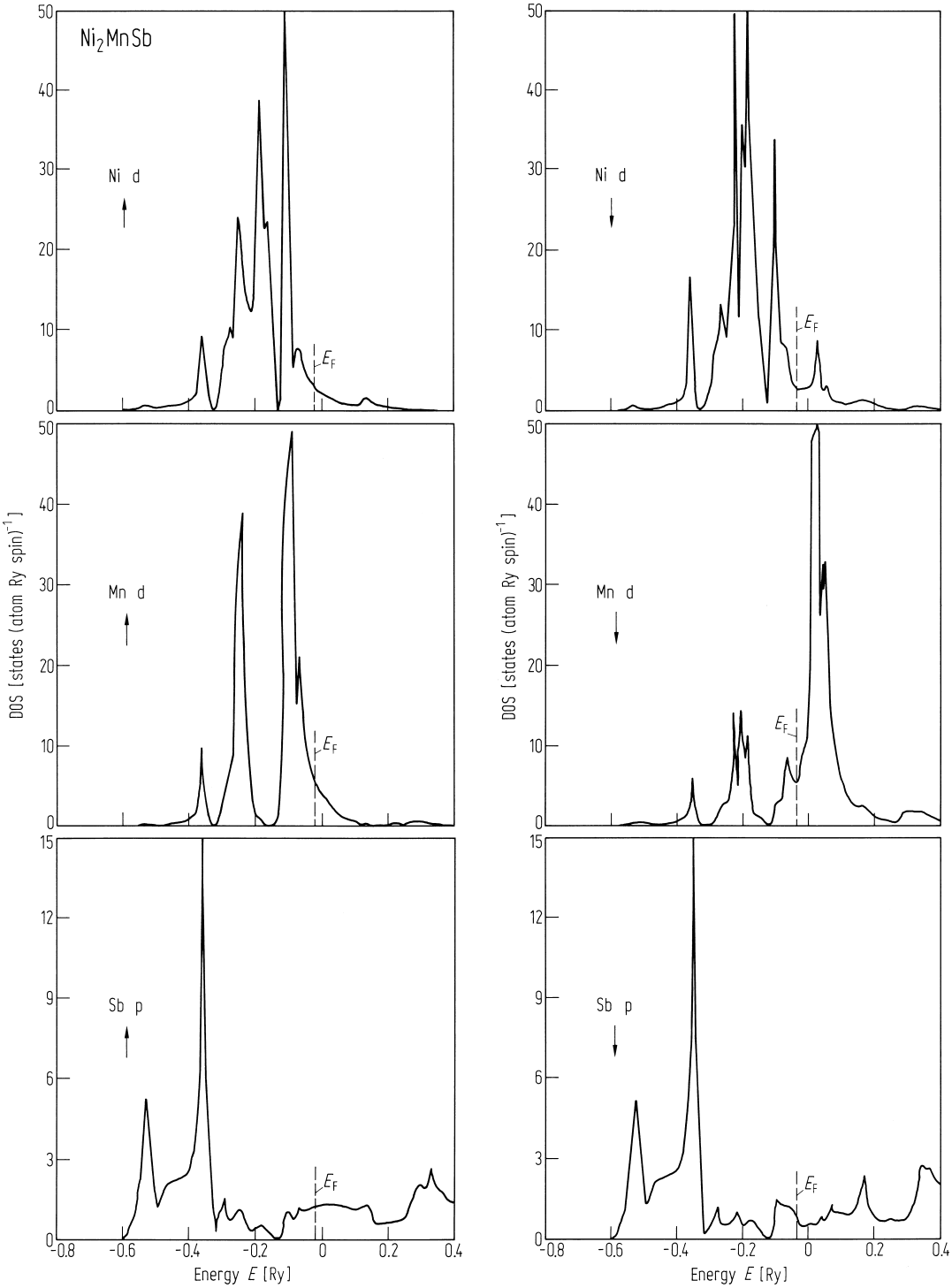

Fig. 516. Ni-d, Mn-d, and Sb-p projected densities of states for Ni_2MnSb [88D1].

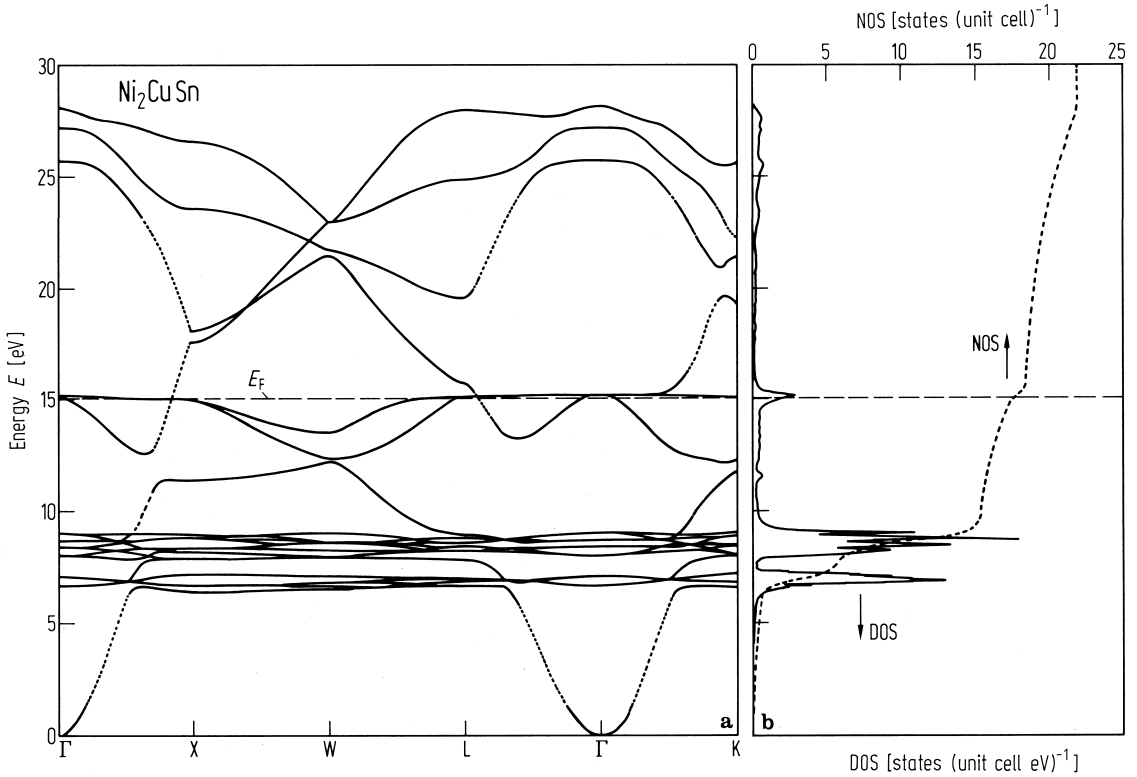

Fig. 517. (**a**) Band structure along the Γ-X-W-L-Γ-K directions in the Brillouin zone and (**b**) corresponding DOS, NOS for Ni_2CuSn compound ($L2_1$ phase). The horizontal line indicates the position of the Fermi level E_F [92D1].

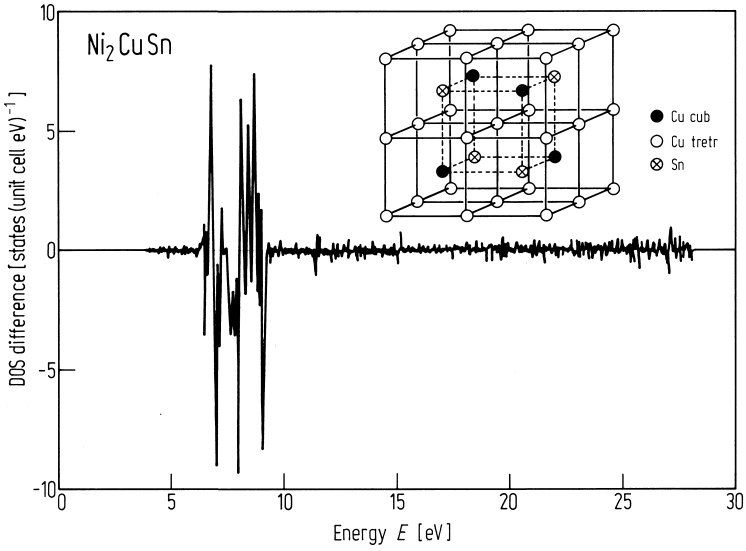

Fig. 519. Difference DOS between densities of states for Ni_2CuSn with $L2_1$ structure and a hypothetical structure. The inset shows the crystal structures. In $L2_1$ and our hypothetical structure the Cu atom occupies cubic position and tetrahedral position respectively. The Sn site is the same in both cases [92D1].

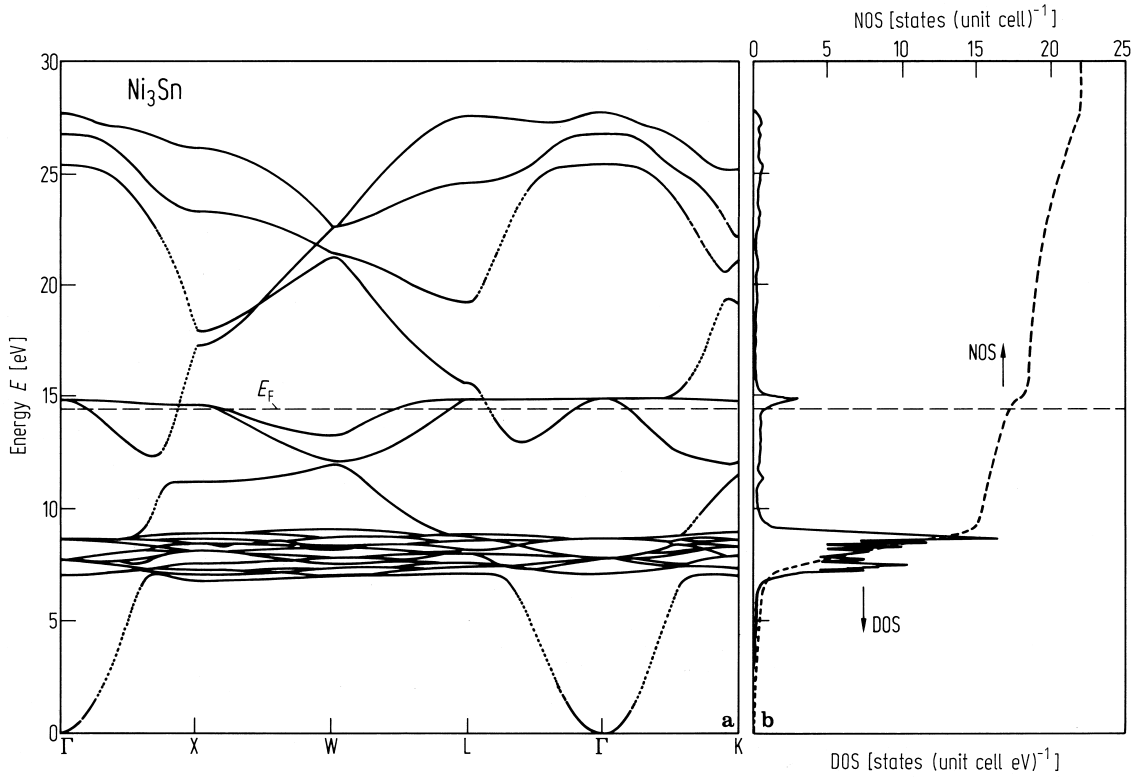

Fig. 518. (**a**) Band structure along the Γ-X-W-L-Γ-K directions in the Brillouin zone and (**b**) corresponding DOS, NOS for Ni_3Sn compound (DO_3) phase. The horizontal line indicates the position of the Fermi level E_F [92D1].

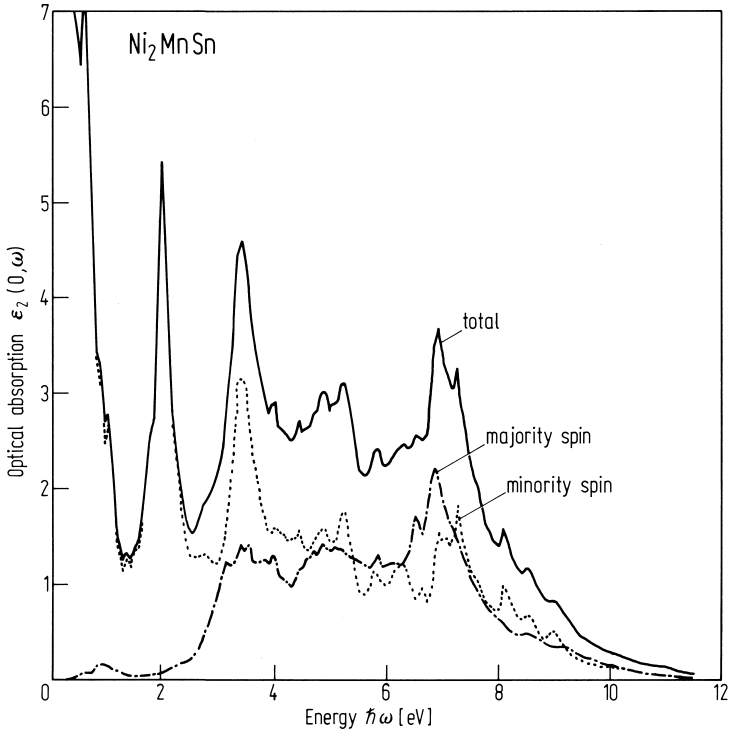

Fig. 521. Theoretical optical absorption spectrum $\varepsilon_2(0,\omega)$ for Ni_2MnSn (full curve). The contributions from the majority- and minority-spin bands are indicated by chain and dotted curves respectively [83K6].

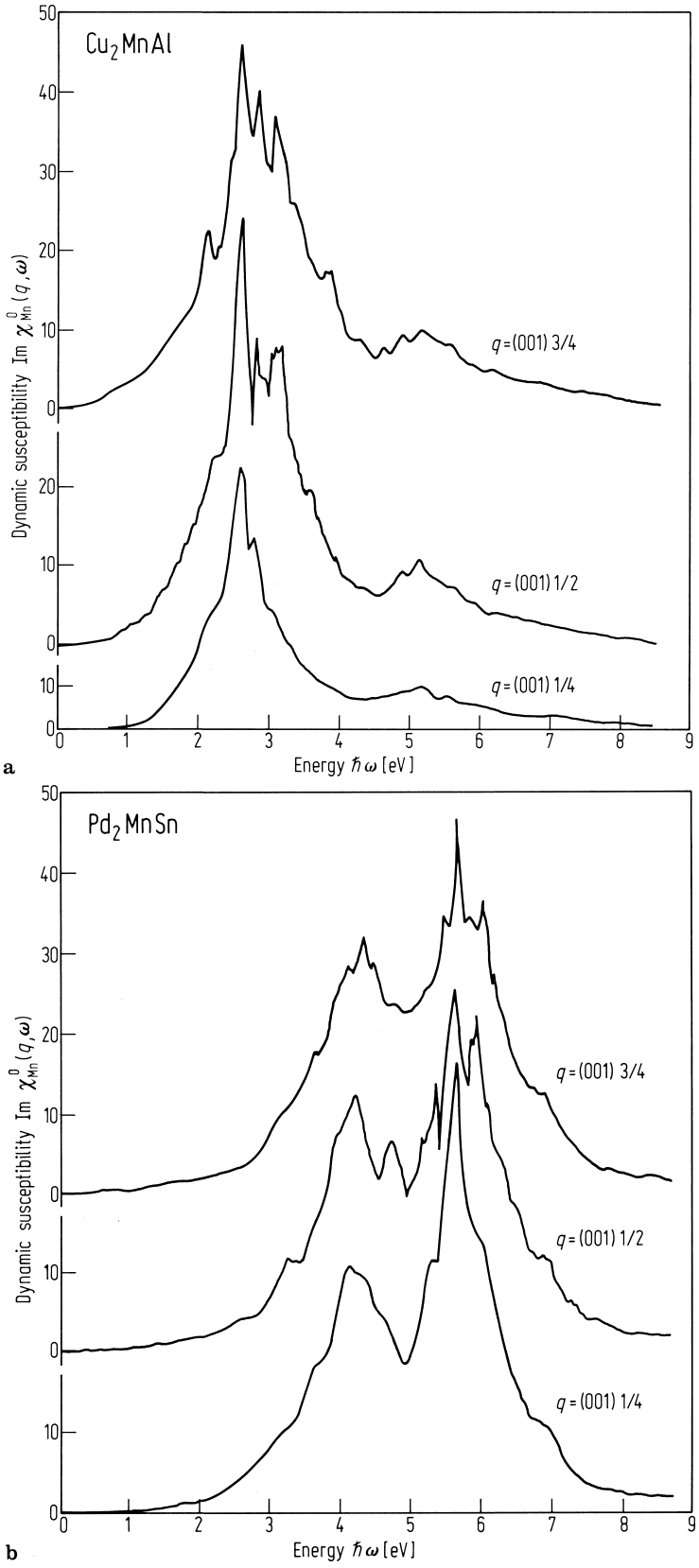

Fig. 520. Imaginary parts of the unenhanced dynamic susceptibility of (**a**) Cu_2MnAl and (**b**) Pd_2MnSn, only due to the diagonal terms of the d-electronic spin-flip excitations of Mn [83K5].

Figs. 522, 523. Partial optical absorption spectra which contribute dominantly to the structures of $\varepsilon_2(0,\omega)$ in Fig. 521 in the minority-spin band (Fig. 522) and in the majority-spin band (Fig. 523). Interband transitions from the initial bands to the final bands are identified by different curves with the respective final band numbers [83K6].

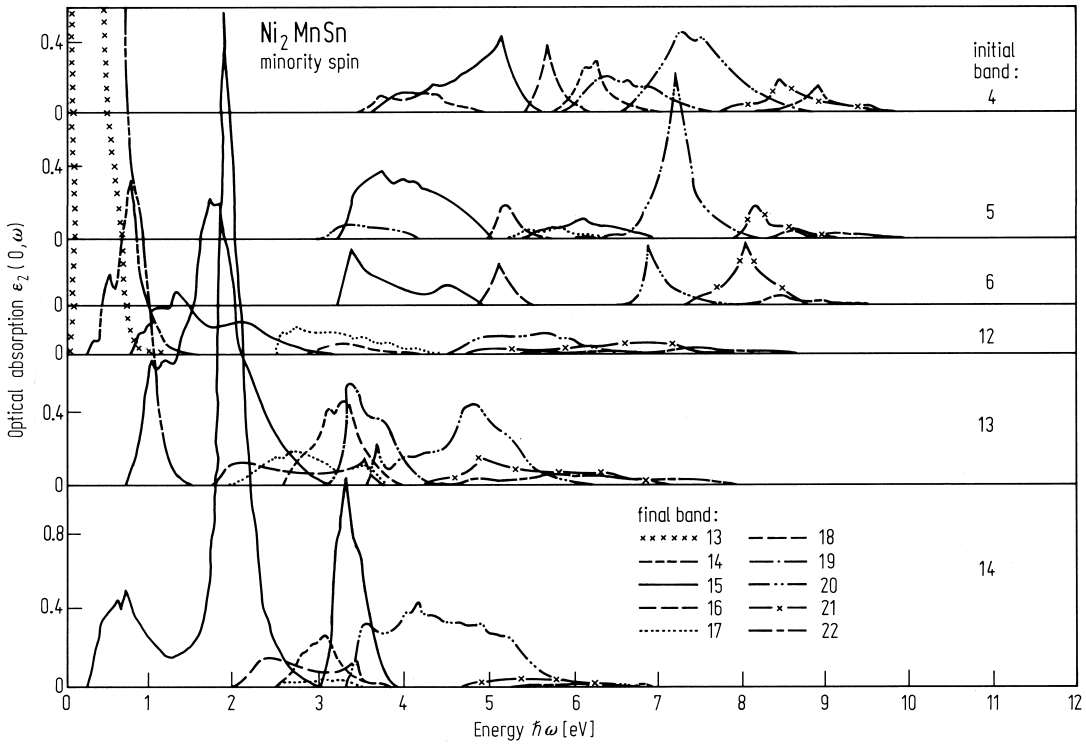

Fig. 522.

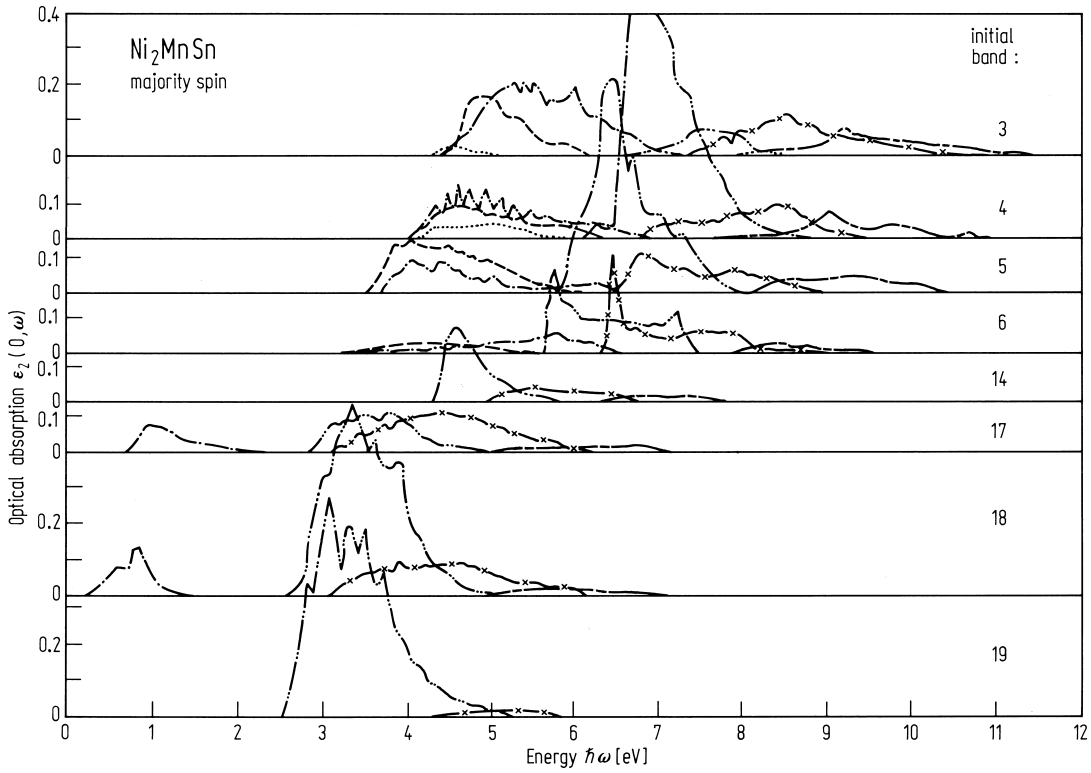

Fig. 523.

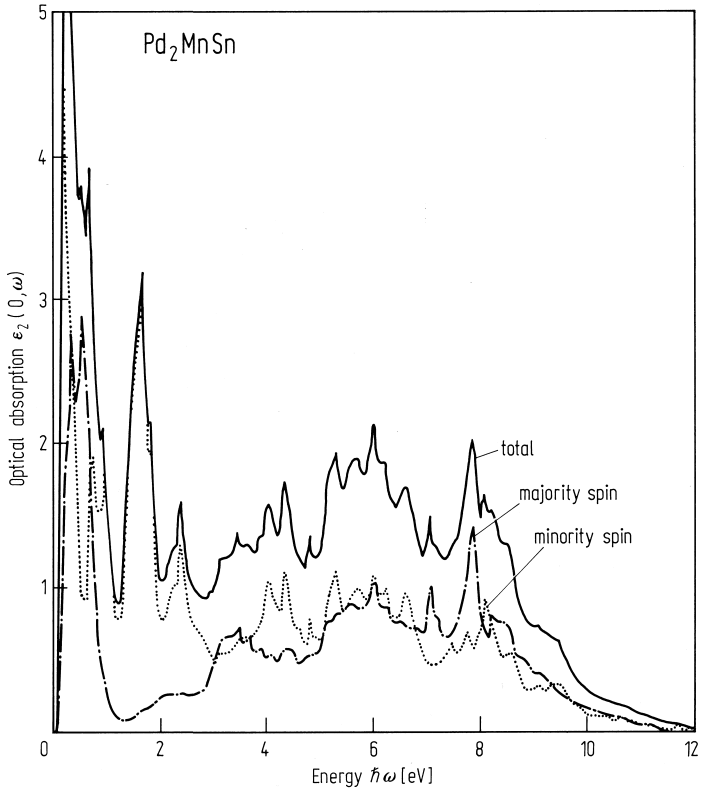

Fig. 524. Theoretical optical absorption spectrum $\varepsilon_2(0,\omega)$ for Pd_2MnSn (full curve). The contributions from the majority- and minority-spin bands are indicated by the chain and dotted curves respectively [83K6].

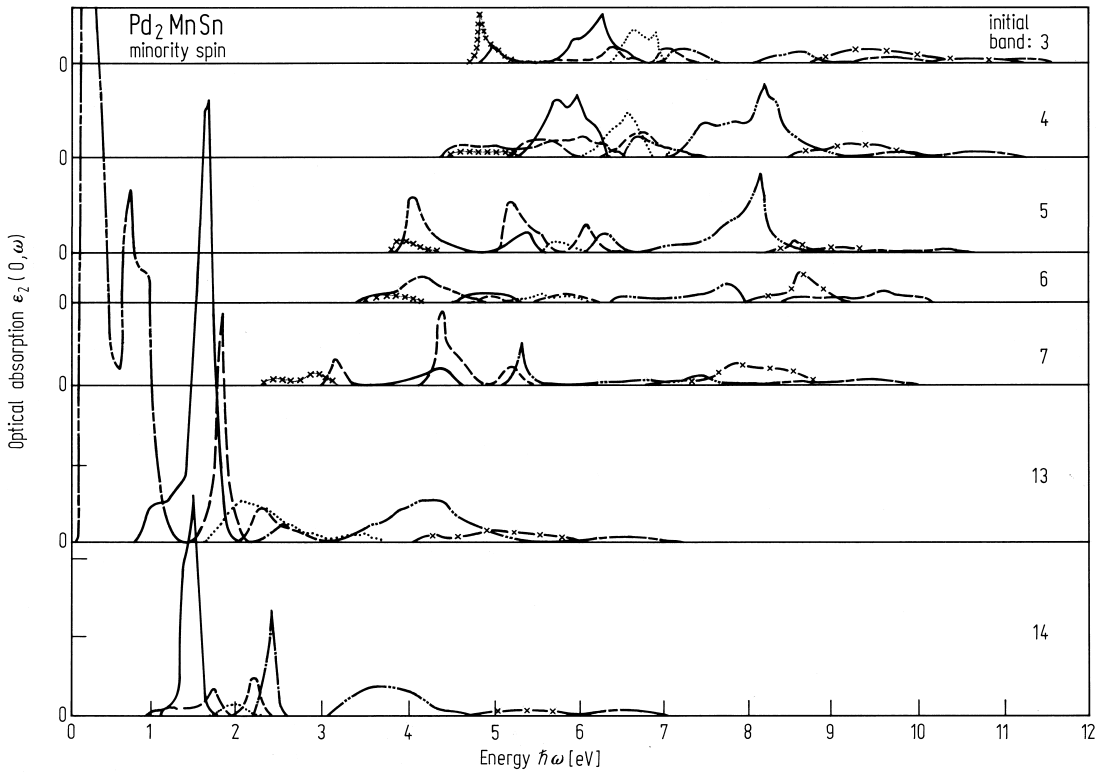

Fig. 525. Partial $\varepsilon_2(0,\omega)$ in Fig. 524 for the minority spin-band. Notation as in Fig. 522 [83K6].

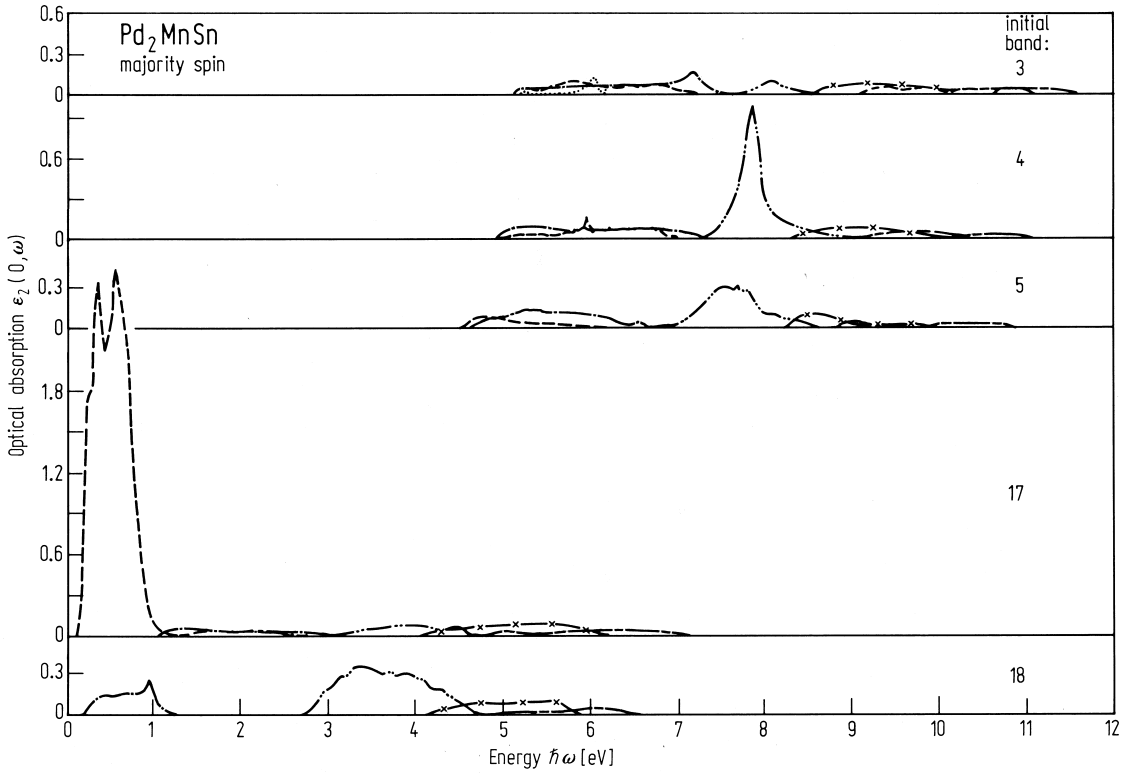

Fig. 526. Partial $\varepsilon_2(0,\omega)$ which contribute dominantly to the structures of $\varepsilon_2(0,\omega)$ in Fig. 524 for the majority-spin band. Notation as in Fig. 522 [83K6].

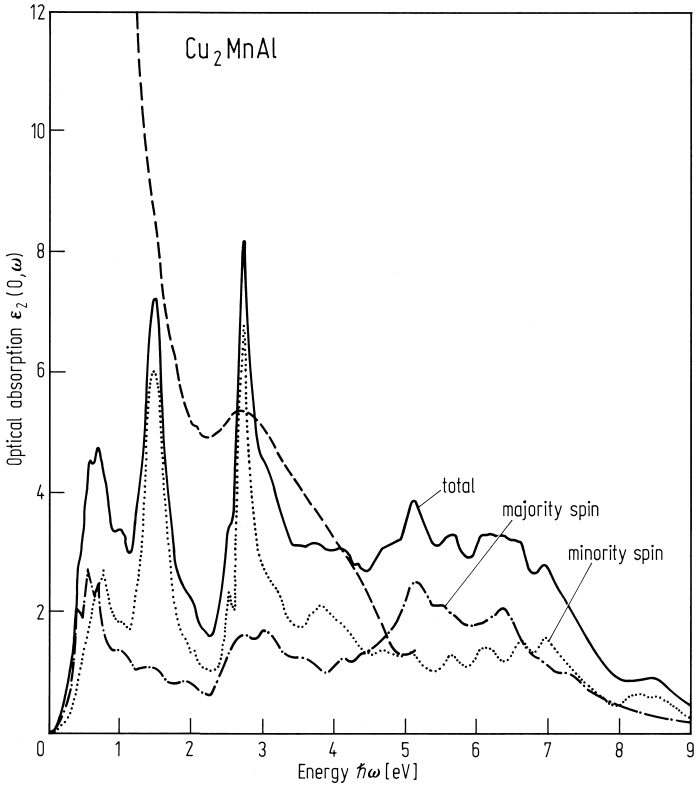

Fig. 527. Theoretical optical absorption spectrum $\varepsilon_2(0,\omega)$ for Cu_2MnAl (full curve). The contributions from the majority- and minority-spin bands are indicated by chain and dotted curves respectively [83K6]. Dashed curve: experimental results of [75M1].

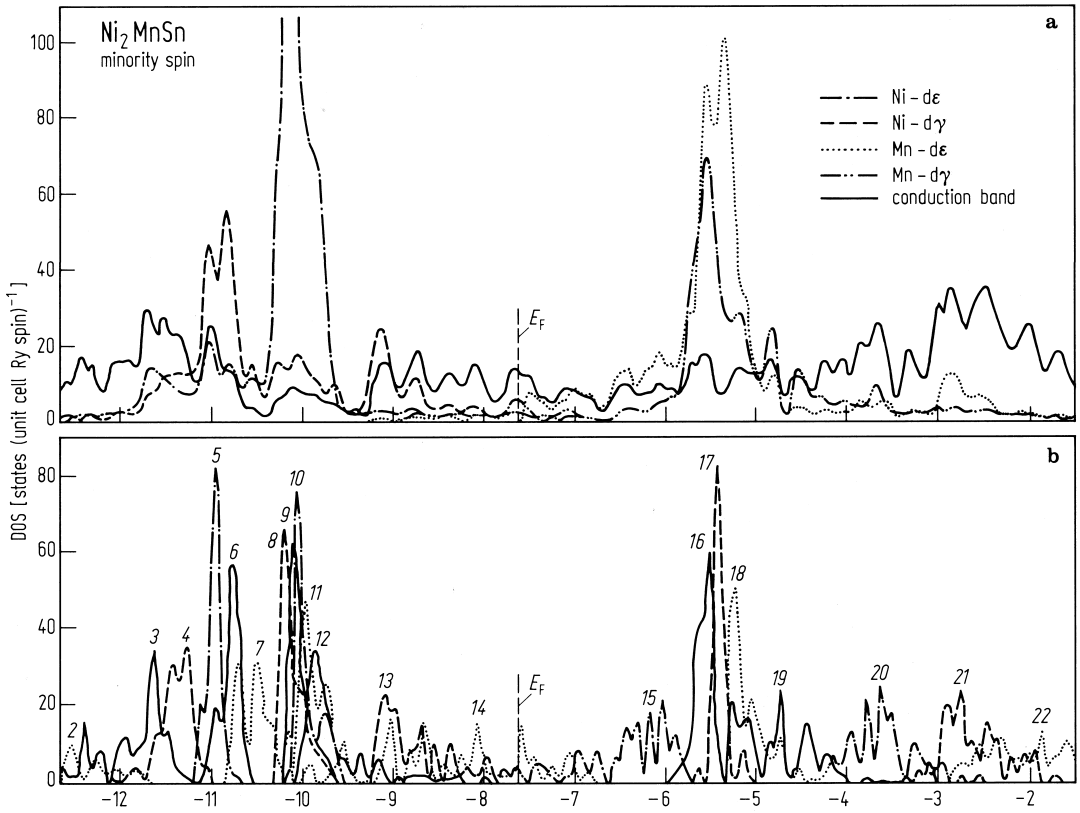

Fig. 528. For caption see p. 340.

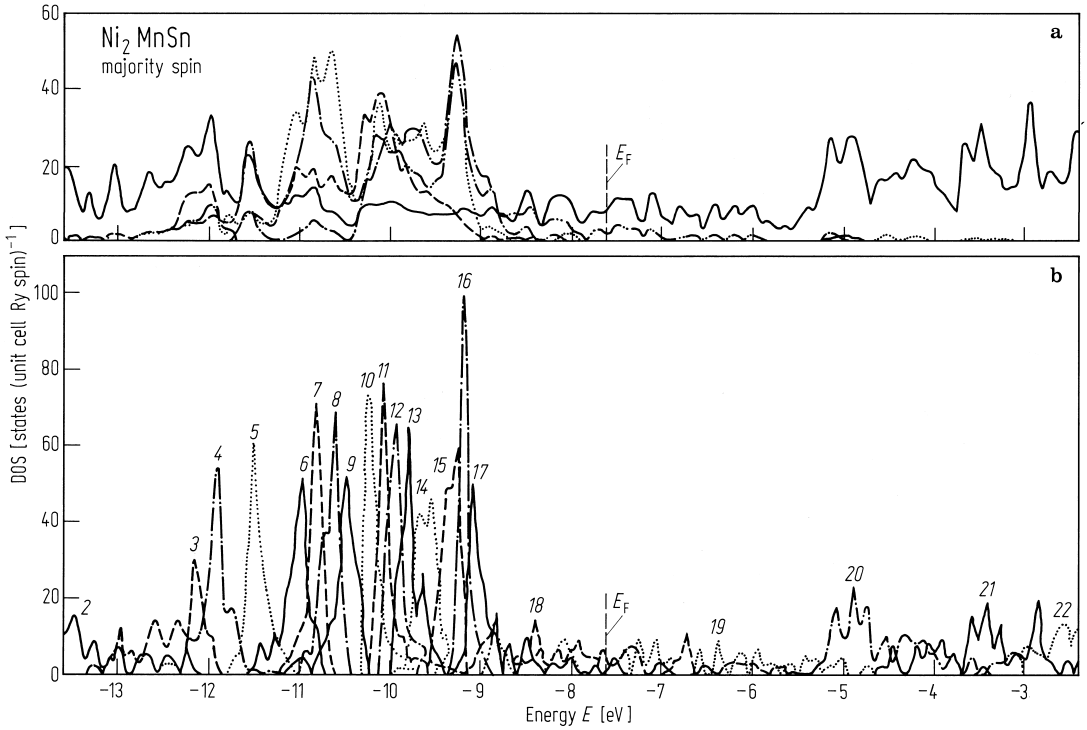

Fig. 529. For caption see p. 340.

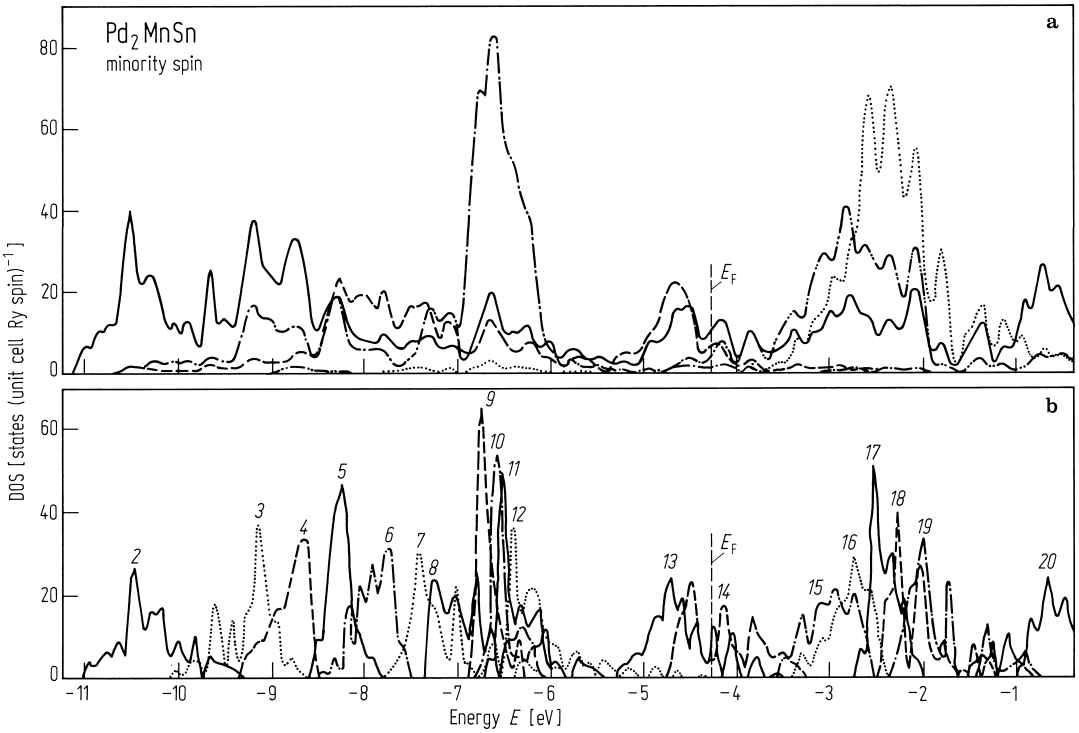

Fig. 530. For caption see p. 340.

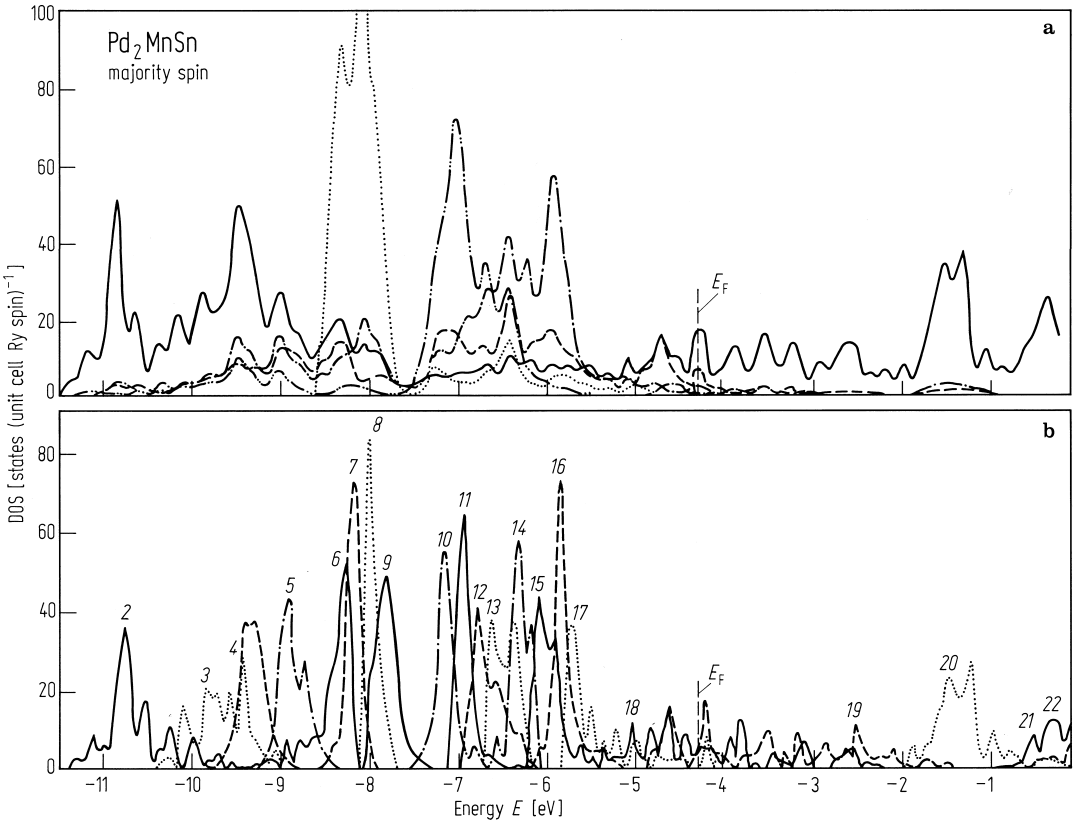

Fig. 531. For caption see p. 340.

Figs. 528-531. Partial density of states in the minority-spin band (Fig. 528) and the majority-spin band (Fig. 529) of Ni_2MnSn. (**a**) Partial densities of states for the d states of Ni (dε, dγ) and Mn (dε, dγ) and the conduction state (OPW), (**b**) partial densities of states for each band: in this case the notations *1*, *2*, *3*, etc. represent band indices. The Fermi level E_F is indicated by the vertical line. Fig. 530 shows the minority-spin band and Fig. 531 the majority-spin band of Pd_2MnSn [83K6].

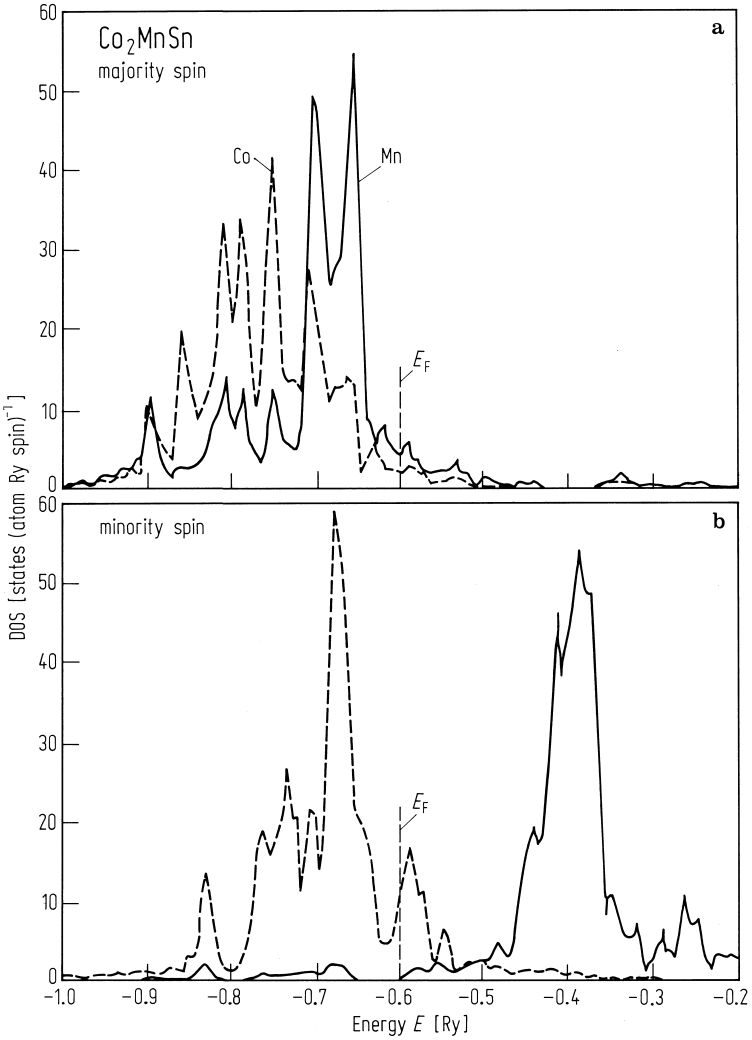

Fig. 532. d-band DOS for (**a**) majority spins and (**b**) minority spins of the constituent atoms of Co_2MnSn. Full curve Mn, broken curve Co [83I1].

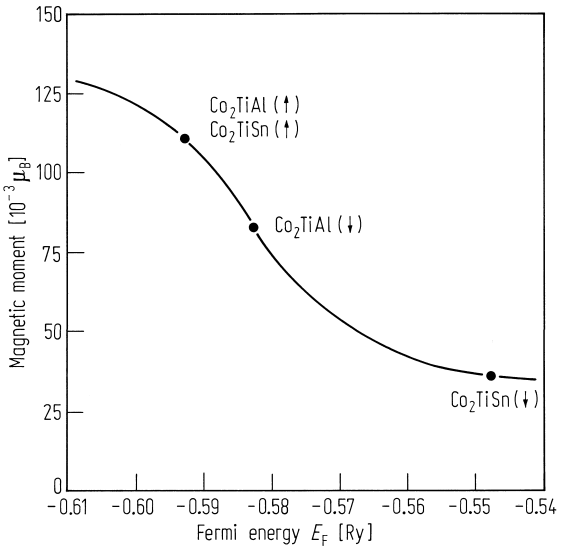

Fig. 533. Contributions of the orbital angular momentum for the majority (↑) and minority (↓) spins to the magnetic moment. This curve is obtained from the DOS of the minority spins of Co_2MnSn [83I1].

$C1_bXYZ$ X = 3d; 5d, Y = 3d

X = 8A: Co, Ni
Y = 7A: Mn
Z = 5B: Sb

XMnSb

Exchange constants and Curie temperatures have been calculated. CoMnSb is shown to be a half-metallic ferromagnet.

Table 113. Calculated exchange constants J_1 and J_2 and paramagnetic Curie temperatures Θ_{calc} for some Heusler $L2_1$ and $C1_b$ compounds [84K1].

		J_1 [meV]	J_2 [meV]	Θ_{calc} [K]	T_C (exp) [K]
Co_2MnAl	($L2_1$)	0.840	0.062	808	697
Cu_2MnAl	($L2_1$)	0.333	0.329	690	630
Pd_2MnSn	($L2_1$)	0.178	– 0.019	285	189
CoMnSb	($C1_b$)	0.431	0.120	600	490
NiMnSb	($C1_b$)	0.307	0.218	770	720
PtMnSb	($C1_b$)	0.281	0.139	650	575

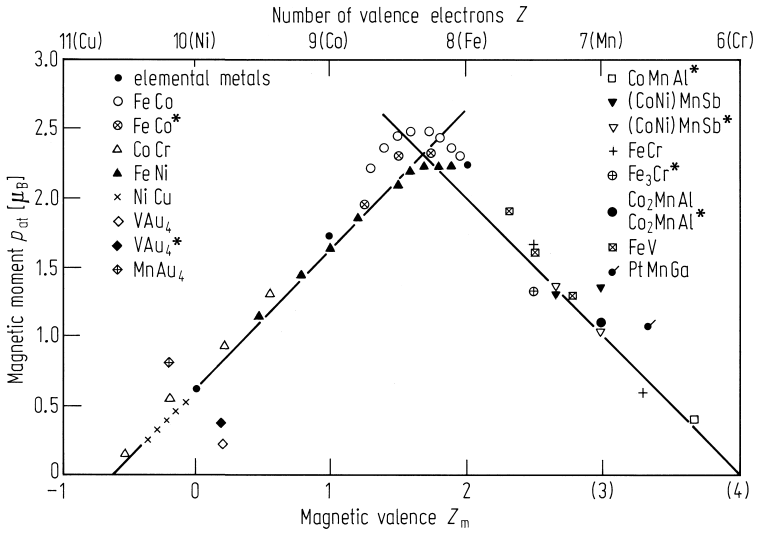

Fig. 534. Generalised Slater-Pauling curve. Magnetisation per alloy atom vs. magnetic valence Z_m in the left part, vs. average number of valence electrons, Z in the right part [84K1].

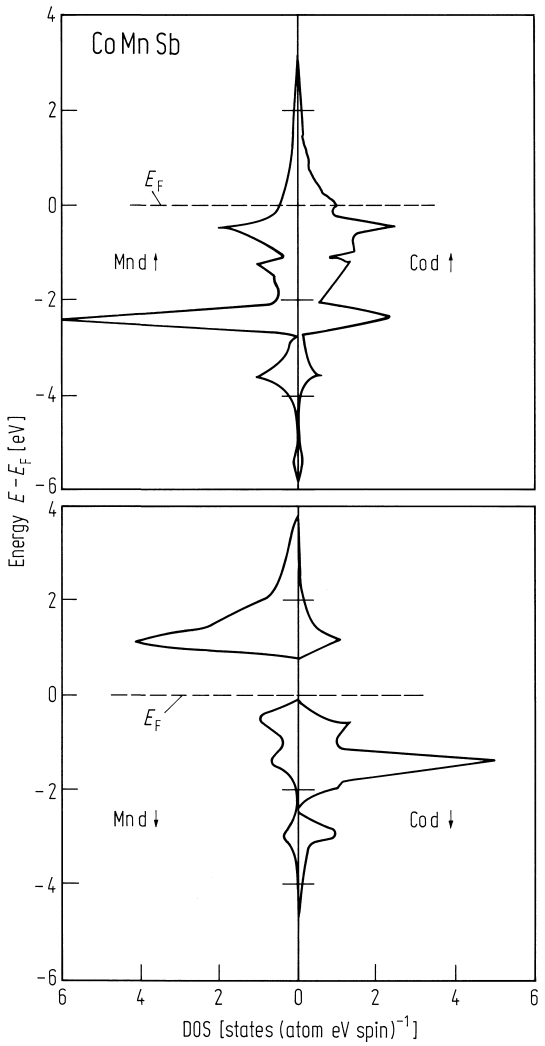

Fig. 535. Majority-spin d-density of state (DOS) of Mn and Co, minority d-DOS of Mn and Co [84K1].

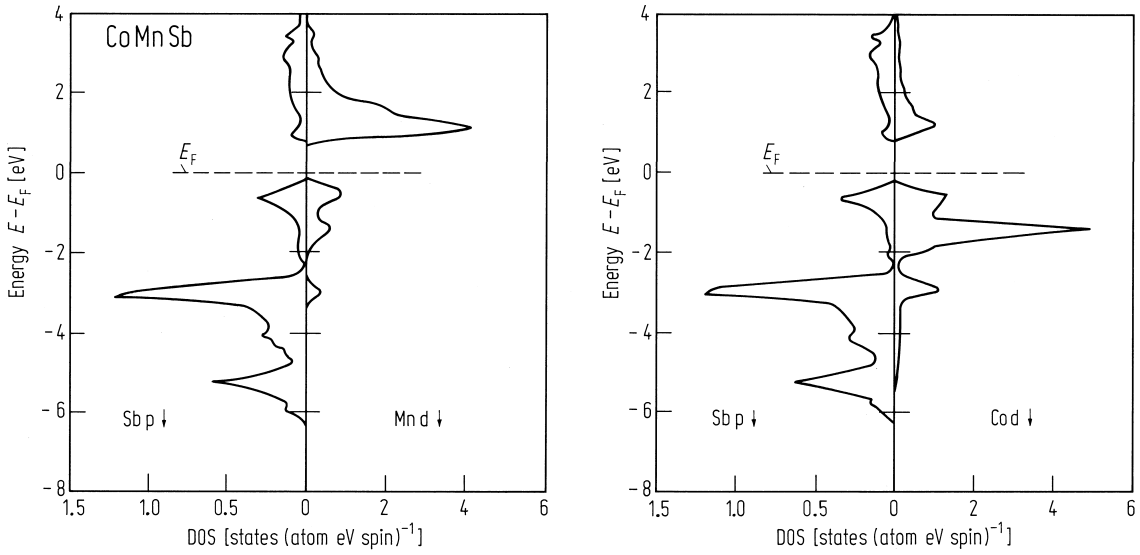

Fig. 536. Minority-spin p-density of state (DOS) for Sb compared with minority d-DOS of Mn and of Co [84K1].

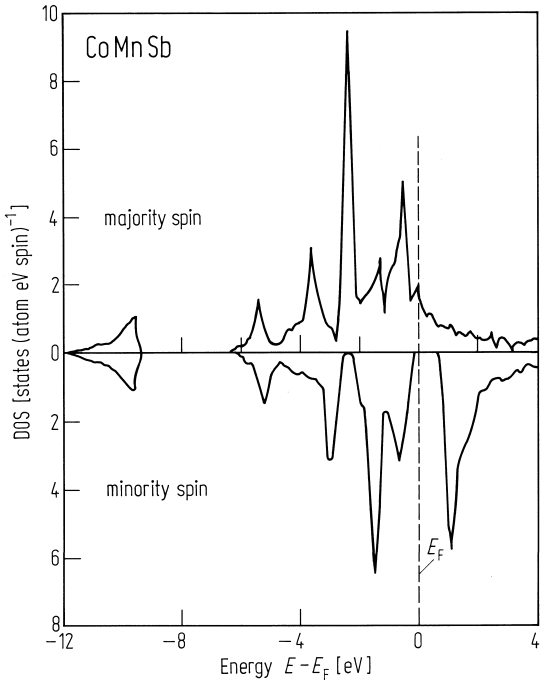

Fig. 538. Total majority spin and minority spin density of states of CoMnSb [84K1].

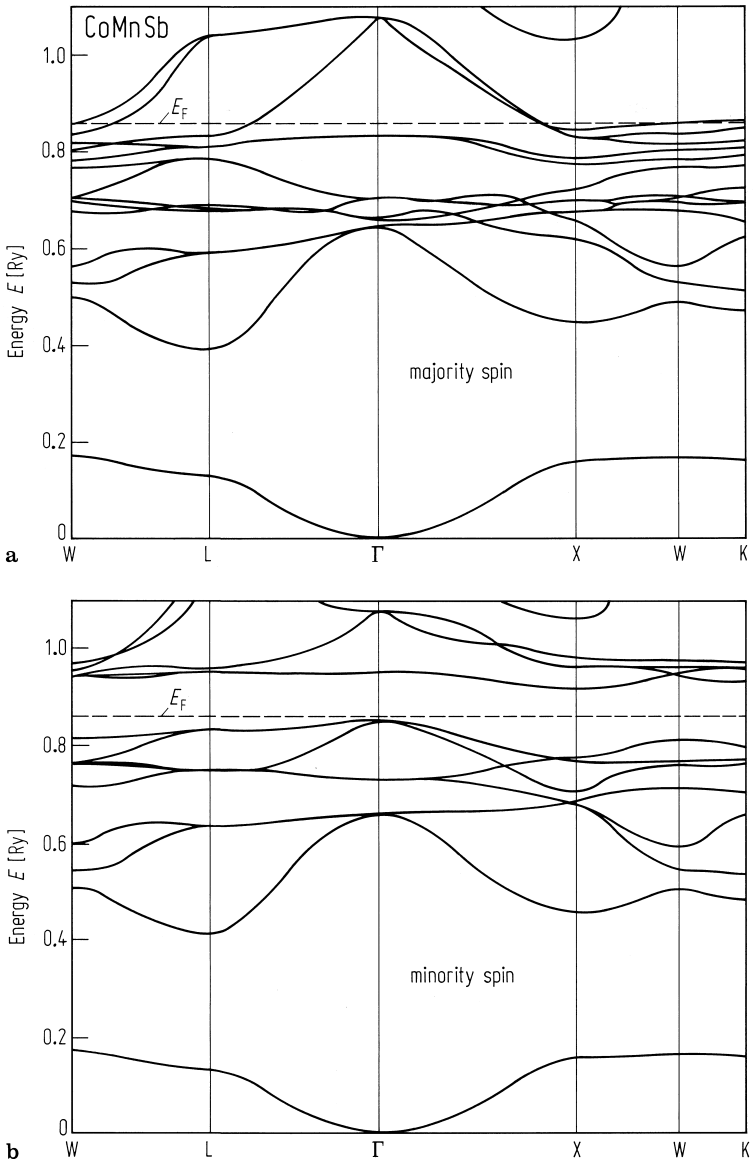

Fig. 537. (**a**) Band structure of majority-spin electrons; (**b**) or minority-spin electrons of CoMnSb [84K1].

1.5.5.9.2 Cohesion and phase transitions

The conduction electron concentration strongly influences not only the electrical and magnetic properties but also the type and degree of atomic order and phase stability. Ni_2MnGa is an example of a system which undergoes a cubic to tetragonal phase transition which is believed to be a band Jahn Teller effect. The effects of electronic band structure on the local atomic order has been calculated for Cu_2NiZn systems and the Ni_2YAl series.